Available online at www.sciencedirect.com
ScienceDirect
Journal of the European Ceramic Society 29 (2009) 2517–2526
www.elsevier.com/locate/jeurceramsoc

The effect of silica doping on neodymium diffusion in yttrium aluminum garnet ceramics: implications for sintering mechanisms

R. Boulesteix [a], A. Maître [a,*], J.-F. Baumard [a], Y. Rabinovitch [b], C. Sallé [b], S. Weber [c], M. Kilo [d]

[a] *Laboratoire Science des Procédés Céramiques et de Traitements de Surface, UFR Sciences et Techniques, UMR CNRS 6638, 123 Avenue Albert-Thomas, 87060 Limoges Cedex, France*
[b] *CILAS, Ester Technopôle BP 76923, 87069 Limoges Cedex, France*
[c] *Laboratoire de Physique des Matériaux, Ecole des Mines, UMR CNRS 7556, Parc de Saurupt, 54042 Nancy Cedex, France*
[d] *TU Clausthal, Institut für Metallurgie, Robert-Koch-Straße 42, 38678 Clausthal-Zellerfeld, Germany*

Received 27 November 2008; received in revised form 23 February 2009; accepted 3 March 2009
Available online 1 April 2009

Abstract

The Nd^{3+} cation diffusion into transparent polycrystalline YAG ($Y_3Al_5O_{12}$) was investigated as a function of temperature and silica content. Thin neodymium oxide layers were deposited on sintered YAG substrates prior to annealing under air at temperatures from 1400 to 1600 °C. Bulk and grain boundary neodymium diffusion coefficients were measured by secondary ion mass spectrometry. The experimental results show that silica addition increases the diffusivity of Nd^{3+} by a factor 10 whatever the diffusion path, probably as a result of extrinsic point defects formation, especially rare-earth vacancies.

The experimental diffusion data were used to elucidate the sintering mechanism of Nd:YAG ceramics in the temperature range 1450–1550 °C. Firstly, it appeared that the intermediate stage of solid-state sintering should be controlled by the rare-earth diffusion along the grain boundary with an activation energy of about 600 kJ mol^{-1}. Secondly, grain growth mechanism at the final stage of liquid-phase sintering was investigated for silica-doped Nd:YAG samples. Thus, the grain growth should be limited by the reaction at interfaces at a temperature lower than 1500 °C, with an activation energy of about 880 kJ mol^{-1}. At higher temperature, it seems to be limited by the ionic diffusion through the intergranular liquid phase, with an activation energy of 250 kJ mol^{-1}.

Keywords: YAG; SiO_2; Diffusion; Sintering; Grain growth

1. Introduction

Neodymium-doped yttrium aluminum garnet (*i.e.* $Y_{3-x}Nd_xAl_5O_{12}$) is widely used for laser applications. Since the first demonstration of Nd:YAG ceramic laser oscillation in 1995 by Ikesue et al.,[1] significant progress in transparent YAG ceramics has been made. Nowadays, polycrystalline YAG lasers and numerous other transparent ceramics are commercially available with various shapes and doping levels. During the last decade, YAG has proven to be a very good solid state laser host material, in particular for power applications thanks to its good optical and thermomechanical properties.[2–4] In comparison to single-crystals, polycrystalline YAG made by a ceramic process shows numerous advantages. It requires a relatively low sintering temperature ($T \geq 1700$ °C) and large parts can be manufactured in reduced time by conventional processes leading to more and more powerful lasers.[5–8]

Otherwise, the sintering of ceramics as well as other kinetic processes (creep, solid-state reaction, etc.) is usually governed by the matter transport which requires the motion of the ionic species in the volume or along the grain boundaries of polycrystals. In this context, the densification of ceramics is usually controlled by the slowest ionic species in the bulk or along the grain boundaries. In the case of the YAG sintering, the rate-limiting diffusion step should be that of the rare-earth element (Y^{3+} or dopant as Yb^{3+}, Nd^{3+}, Dy^{3+}, La^{3+}) because of its large cationic radius and mass.[9] The diffusion of the rare-earth element (REE) into polycrystalline YAG has been studied from diffusion concentration profiles which were obtained by SIMS[9,10] or RBS techniques.[11] From these stud-

* Corresponding author. Tel.: +33 5 55 45 74 63; fax: +33 5 55 45 75 86.
E-mail address: alexandre.maitre@unilim.fr (A. Maître).

0955-2219/$ – see front matter © 2009 Elsevier Ltd. All rights reserved.
doi:10.1016/j.jeurceramsoc.2009.03.003

ies, it appeared that the volume diffusion coefficients for all the rare-earth elements were quite similar, showing up the role of REE as tracers for yttrium ion diffusion.[9,10,12] It was also confirmed that activation energies for the cation volume diffusion (≈500–600 kJ mol^{-1}) were much higher than those reported for oxygen (≈300–350 kJ mol^{-1}) in the yttrium aluminum garnet lattice.

From literature, no previous work has been reported concerning the effect of silica addition on the rare-earth ion (*e.g.* Nd^{3+}) grain boundary or volume diffusion in YAG. Nevertheless, it is well known that the use of sintering aids (SiO_2, MgO)[13,14] is required to reach fully dense and transparent YAG ceramics by removing the microstructural heterogeneities such as pores and secondary phases.[15] According to several previous papers,[13–16] the effect of the sintering aids should be correlated to the enhancement of the rare-earth grain boundary diffusion due to the occurrence of secondary phases during sintering and/or the decrease of the grain boundary energy. In this context, Sallé and co-workers[17] showed the presence of a liquid-phase sintering when silica was introduced in the reactive oxides mixture. The liquid phase results from the reaction between YAG and silica and should have an eutectic composition in Y_2O_3–Al_2O_3–SiO_2 system.[17] It has been also reported in the literature[18] that the effect of silica addition should be linked to a solid solution formation by substitution of Al^{3+} by Si^{4+} in tetrahedral sites:

$$SiO_2 + \frac{5}{6}Al_{Al}^{\times} + \frac{1}{2}Y_Y^{\times} \rightarrow Si_{Al}^{\bullet} + \frac{1}{3}V_Y''' + \frac{1}{6}Y_3Al_5O_{12} \qquad (1)$$

According to Eq. (1), one expects that the formation of Y^{3+} vacancies enhances the lattice diffusion coefficient and, consequently, affects the YAG densification mechanism. However, Si^{4+} ions are slightly smaller than Al^{3+} (0.026 versus 0.039 nm[19]) leading to elastic distortions in YAG lattice. As a consequence, only a small quantity of silica can be expected to dissolve in pure YAG during the sintering.

The present study is then focused on the role of the silica on the Nd^{3+} grain boundary or volume diffusion during sintering. The diffusion profiles were obtained by using the SIMS method which made the diffusion analyses possible at low concentrations of rare-earth element ions. The diffusion coefficients (D_v, D_{gb}) determined during this work were compared to the kinetical data deduced independently from the analysis of the densification and the grain growth mechanism of YAG with or without silica additions.

2. Experimental procedure

2.1. Preparation of Nd_2O_3-coated YAG samples

The measurements of the neodymium diffusion were performed from YAG dense substrates covered by thin and pure neodymium oxide coatings. The corresponding experimental procedure is summarized in Fig. 1.

At first, polycrystalline YAG substrates were manufactured according to the following process. Submicrometer α-Al_2O_3 (purity >99.99%, Baïkowski, France) and Y_2O_3 powders (purity >99.99%, Alfa Aesar, Germany) were mixed together in stoichiometric proportions to form $Y_3Al_5O_{12}$. Nanosized silica (purity >99.8%, Alfa Aesar) was added in three different concentrations: 0, 0.05 and 0.3 wt.%. After uniaxial pressing and calcination to remove organic residues, pellets nominally 20 mm in diameter by 5 mm high were sintered under vacuum at 1700 °C for 3 h to provide fully dense materials. The sintered YAG samples showed an average grain size ranging between 4 and 10 μm as a function of the silica content. More particular, it appears that the higher the silica content, the lower the grain size. The thin substrates for the deposition step were prepared by cutting thin slices with a diamond saw (1 mm thick by a section of 20 mm). One side of these slices was then polished by using different diamond sprays of 6, 3 and 1 μm.

At second, the deposition step of a neodymium oxide precursor was based on the polymeric precursor method (*i.e.* a sol–gel process) which is widely used to obtain oxides thin films.[20] Hexahydrated neodymium nitrate (purity ≥99.9%, Alfa Aesar) was mixed with monohydrated citric acid (purity ≥99%, Fisher Chemicals, UK) and dissolved in a solvent containing ethylene glycol (purity ≥99%, Fisher Chemicals) and deionized water, with the molar ratio 1:1.67:10:5.55. This solution was then stirred and heated at 90 °C for about 2 h. Neodymium citrate was then formed by reaction between citric acid and neodymium

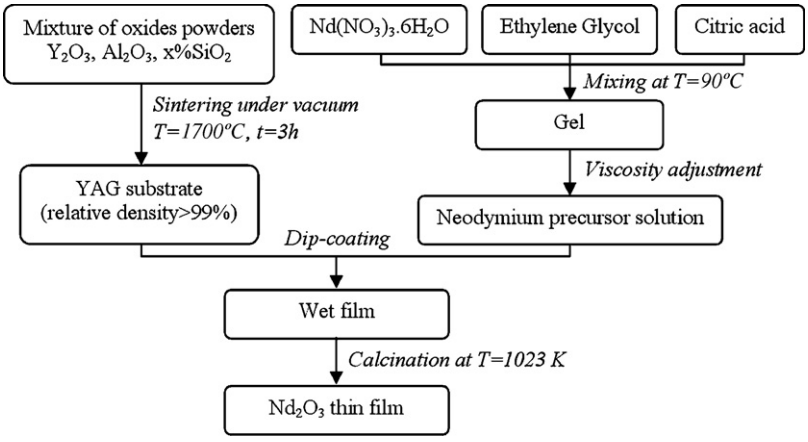

Fig. 1. Scheme of the dip-coating process leading to Nd_2O_3 thin films on YAG substrates.

nitrate. Thanks to heating, neodymium-based citrates underwent a polyesterification reaction in presence of ethylene glycol which leads to a viscous gel. The gel viscosity was controlled by a shear rate-controlled rheometer (Carri-Med CSL100, Dorking, UK) and was fixed to 50 mPa s by water addition. The covering process of YAG substrates was performed thanks to a dip-coating device at a withdrawal rate of 0.2 mm s^{-1}. Samples were then heat-treated in air at 800 °C for 1 h. The heating rate and the cooling rate were fixed to 1 °C and 4 °C.min^{-1}, respectively.

X-ray diffraction analysis (D5000 Siemens, CuKα radiation, Germany) was carried out from the powder obtained after calcination in air at 800 °C and grinding in an agate mortar. The scanning time and the angular step were fixed to 2 h and 0.04°, respectively. The cross-section of the Nd_2O_3-coated YAG sample was observed by means of scanning electron microscopy (FEG-SEM, JEOL, JSM-7400F, France) and the surface by atomic force microscopy in taping mode (AFM PicoLE, Molecular Imaging Co., Scientec, France).

2.2. SIMS analyses

The diffusion annealings were achieved in air between 1400 and 1600 °C. The annealing time varied between 2 and 145 h as a function of the temperature. Neodymium concentration profiles were determined by secondary ion mass spectrometry (SIMSLAB, VG Instruments, UK). Cs^+ ions (8 kV, 80 nA) were used as primary ion beam. To limit charging effects, an electron flood gun was coupled to the primary beam and samples were previously covered by sputtering with a thin layer of gold. The final crater depth was measured using a profilometer (DEKTAK, Sloan, US) with a 5 nm resolution. Crater area and depth were fixed to 500 μm × 500 μm and 2.5 μm, respectively. The analyzed zone was only 30% of the crater surface to avoid edge effects. Secondary ions (*i.e.* Nd^+, Al^+ or Y^+) were detected with an electron multiplier and the Nd^+/Al^+ intensity ratio was converted as a function of depth using the sputtering time, the final crater depth and assuming a constant sputtering rate. The average grain size of annealed specimens was determined by using optical or scanning electron microscopy (SEM) and image analysis (Scion software, Scion Corp., USA). The equivalent disc diameter was chosen as a parameter for size evaluation. For each sample, average grain size measurement was done over 300 grains which lead to an error of about 2.5%.

3. Results and discussion

3.1. Nd^{3+} diffusion in pure YAG specimens

The presence of the Nd_2O_3 phase in the calcinated powder of neodymium precursor (JCPDS 01-074-2139 file) was evidenced from the X-ray diffraction pattern (Fig. 2). FEG-SEM observations revealed that the dip-coating process led to a 100 nm thick layer (Fig. 3a). This coating appeared to be homogeneous, dense and nanostructured as shown by AFM characterizations (Fig. 3b). From these experiments, it can be deduced that the Nd_2O_3 oxide film should be sufficiently thin and homogeneous to make the diffusion experiments possible.

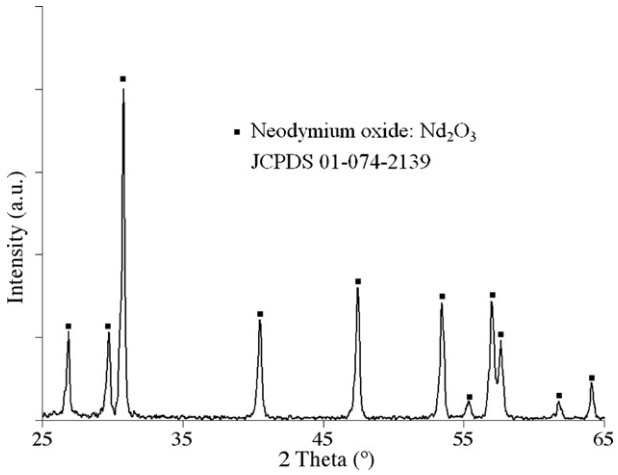

Fig. 2. XRD pattern of the Nd_2O_3 powder issued from the grinding and the calcination treatment of gel at 800 °C for 1 h in air.

Assuming that the analyzed area (300 μm × 300 μm) by SIMS is much larger than the grain size (5–20 μm), the signal intensity was assumed to be proportional to the average neodymium concentration at a given depth. Fig. 4 presents a typical diffusion profile for neodymium into a "pure" polycrystalline YAG sample (*i.e.* prepared without silica addition). This diffusion profile was obtained after annealing in air at 1450 °C for 44 h.

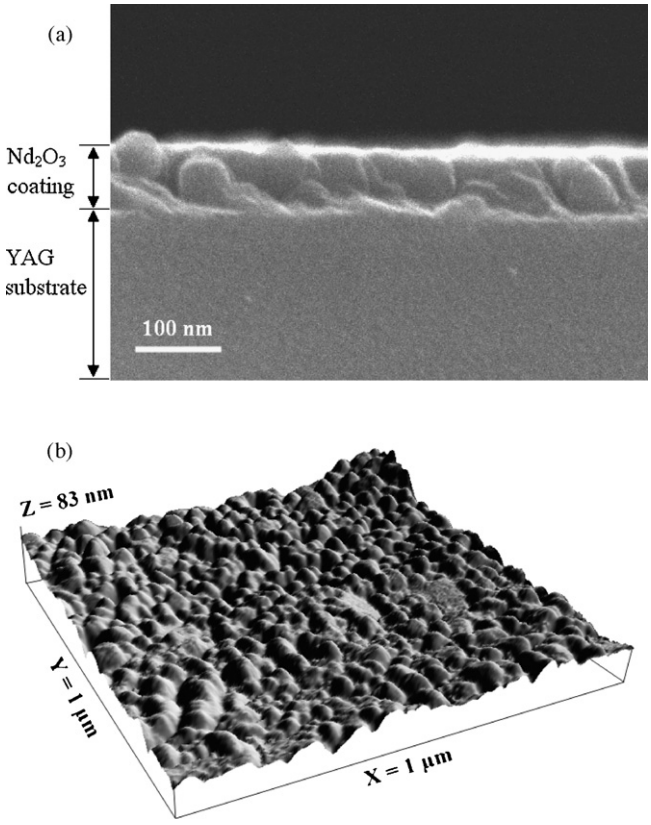

Fig. 3. SEM observation of the cross-section (a) and AFM image of the surface (b) of a Nd_2O_3 coating on YAG substrate after calcination at 800 °C for 1 h in air.

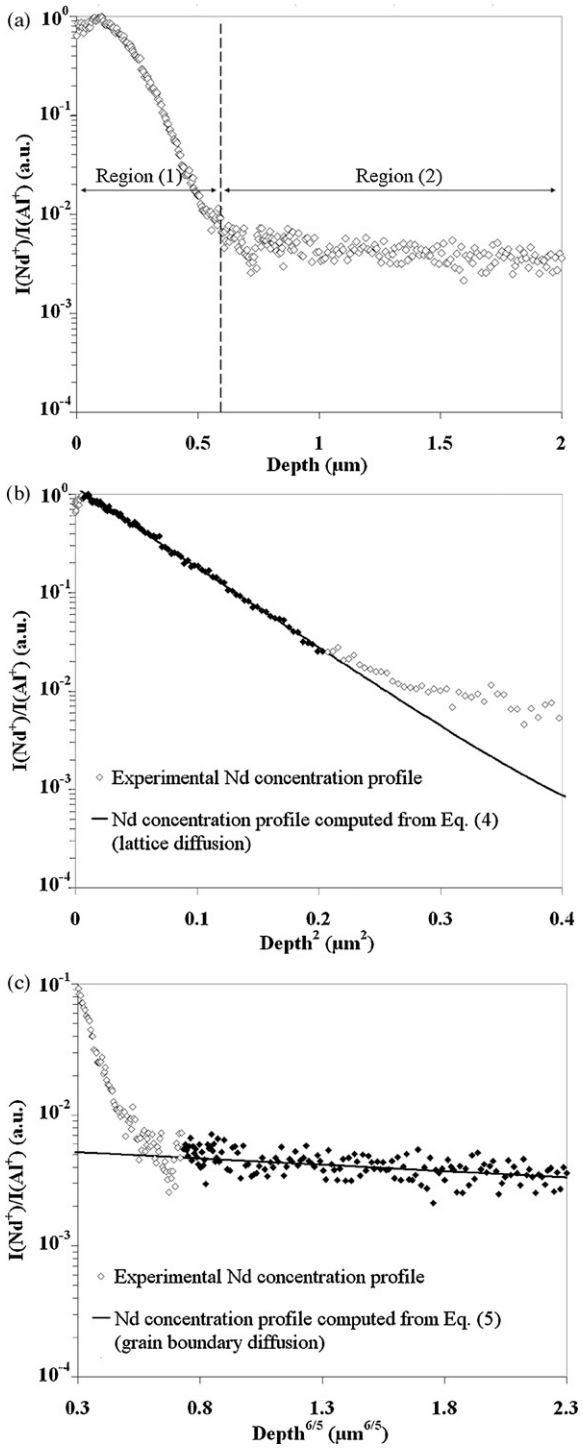

Fig. 4. SIMS diffusion profile of neodymium in "pure" YAG polycrystal treated at 1450 °C for 44 h (a), with experimental and calculated profiles reported for volume diffusion in region 1 (b) and grain boundary diffusion in region 2 (c).

The concentration profile derived from the SIMS pattern was fitted with analytical models to determine the volume (D_v) and the grain boundary diffusion coefficients (D_{gb}). For this study, the diffusion process was analyzed with a one-dimensional diffusion model. From Fig. 4a, it is evident that the penetration profile of neodymium in polycrystalline YAG can be divided in two parts:

- one near the sample surface (penetration depth $x < 0.6\,\mu m$) which corresponds to a rapid decrease of the neodymium concentration. This region, marked 1 in Fig. 4a, is usually attributed to the volume diffusion;
- one away from the surface ($x > 0.6\,\mu m$) which is associated to a linear part. The Nd^{3+} concentration slowly decreases in this region marked as region 2 in Fig. 4a and is linked to the grain boundary diffusion regime.

The bulk diffusion coefficient D_v was determined from the first part of the concentration profiles using the thin-film solution of the Fick's one dimension second law[21]:

$$\frac{I(Nd^+)}{I(Al^+)} = \frac{\alpha}{\sqrt{4\pi D_v t}} \exp\left[-\frac{x^2}{4D_v t}\right] + I_b \quad (2)$$

where α is a constant proportional to the initial amount of diffusing ions in the Nd_2O_3 thin film, t the annealing time, x the penetration depth and I_b the background intensity. The dark line in Fig. 4b is the theoretical concentration profile computed from Eq. (2). The calculation of the volume diffusion coefficient from Eq. (2) shows that the grain boundary transport occurred in the so-called type B kinetic regime ($10\delta < (D_v t)^{1/2} < G/10$), where G is the grain size. Therefore, the grain boundary diffusion coefficients D_{gb} were obtained from linear parts of the penetration profiles (region 2 in Fig. 4a) and the thin films solution established by Le Claire[22]:

$$P = s.\delta.D_{gb} = 0.66\sqrt{\frac{4D_v}{t}}\left[-\frac{\partial \ln(I(Nd^+)/I(Al^+))}{\partial x^{6/5}}\right]^{-5/3} \quad (3)$$

where the Le Claire parameter P depends on the segregation coefficient s of neodymium into YAG and the grain boundary thickness δ. The segregation coefficient is classically reported equal to 1 for self-diffusion.[21] Since both the neodymium coating was thin (*i.e.* the neodymium quantity remained low) and its solubility in YAG was found to be as high as 20 at.% at 1500 °C,[23] it was supposed that no neodymium segregation occurred (*i.e.* $s = 1$) during diffusion annealing. For calculations of D_{gb} coefficient, a grain boundary width δ of 1 nm was assumed. This latter value is commonly in use for polycrystalline YAG.[9,10] Using the Le Claire solution, it was checked that the experimental data plotted versus $x^{6/5}$ yielded a straight line (see Fig. 4c).

A similar procedure was carried out to extract the lattice and grain boundary diffusivities for all the annealing times and temperatures. The whole set of useful diffusion data was reported in Table 1 with relevant details. From these experiments, it was checked that no time dependence occurs in the calculation of D_v parameter. In fact, similar values of $(D_v t)^{1/2}$ were determined for 0.05 wt.% SiO_2-doped samples treated at 1600 °C for different soaking times. Also are presented in Table 1 the final densities and grain sizes. From the comparison of the average grain size for the shortest and the longest diffusion annealing times at different temperatures, it was checked that no significant grain growth occurred.

At first, we have performed diffusion experiments on YAG undoped single-crystals (R60-S grade, FEE GmbH, Germany)

Table 1
Data for calculating bulk and grain boundary diffusion coefficients.

Silica content (wt.%)	Temperature (°C)	Time (s)	Density (g cm^{-3})	Grain size (μm)	D_v (m^2 s^{-1})	$\sqrt{D_v t}$ (nm)	d/10 (nm)	D_{gb} (m^2 s^{-1})
0	1400	522000	4.53	10.4	1.76×10^{-20}	96	1044	9.89×10^{-16}
0	1450	158400	4.53	11.0	6.47×10^{-20}	101	1102	5.10×10^{-15}
0	1500	72000	4.53	11.1	2.39×10^{-19}	131	1112	1.30×10^{-14}
0	1450	158400	4.55	Single-crystal	1.11×10^{-19}	133	–	–
0	1550	10800	4.55	Single-crystal	1.12×10^{-18}	110	–	–
0	1600	7200	4.55	Single-crystal	2.59×10^{-18}	137	–	–
0.05	1400	522000	4.55	9.4	4.58×10^{-20}	155	943	3.17×10^{-15}
0.05	1450	158400	4.55	11.7	8.13×10^{-20}	113	1170	2.31×10^{-14}
0.05	1500	72000	4.55	8.3	3.70×10^{-19}	163	826	3.58×10^{-14}
0.05	1550	10800	4.55	12.5	1.44×10^{-18}	125	1245	2.89×10^{-13}
0.05	1600	3600	4.55	9.8	3.55×10^{-18}	113	980	–
0.05	1600	7200	4.55	10.6	1.82×10^{-18}	114	1062	–
0.3	1400	522000	4.51	3.8	8.26×10^{-20}	208	381	8.32×10^{-15}
0.3	1450	158400	4.51	3.8	3.97×10^{-19}	251	378	5.71×10^{-14}
0.3	1500	72000	4.51	4.2	9.82×10^{-19}	266	418	1.61×10^{-13}
0.3	1550	5400	4.51	4.2	2.36×10^{-20}	113	420	–

which were Nd_2O_3-coated in the same way than YAG polycrystals. Experimental diffusion results were reported in Table 1 and Fig. 5. Thus, a good agreement was obtained between diffusion profiles for single and polycrystalline YAG samples as shown in Fig. 5. Only the tail of the curve ($x > 0.5$ μm) differs due to the effect of grain boundary diffusion in polycrystalline YAG. Moreover, the experimental diffusion profile for single-crystal fits well the calculated curve for the volume diffusion in polycrystal, what suggests that the bulk consists in the sole diffusion path for single-crystal.

For the neodymium diffusion in "pure" YAG polycrystal, the calculated values of D_v and D_{gb} were reported as a function of reciprocal temperature in Fig. 6a. From this plot, the diffusivities were obtained in the form $D = D_0 \exp(-Q/RT)$ where D_0 is the frequency factor, Q the activation energy and R the gas constant:

$$D_v^{Nd} = 2.0 \ \exp(-643 \pm 11\,\text{kJ mol}^{-1}/RT)\,[\text{m}^2\,\text{s}^{-1}] \quad (4)$$

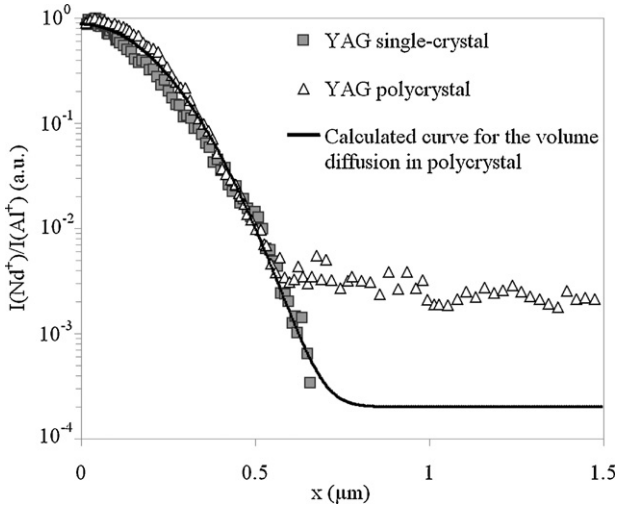

Fig. 5. Experimental diffusion curves for single (closed symbols) and polycrystalline (open symbols) YAG. Theoretical volume diffusion profile was calculated from polycrystalline YAG data (dark line). Samples were Nd_2O_3-coated and annealed at 1450 °C for 44 h in air.

$$D_{gb}^{Nd} = 3.5 \times 10^9 \exp(-637 \pm 90\,\text{kJ mol}^{-1}/RT)[\text{m}^2\,\text{s}^{-1}] \quad (5)$$

Also are reported in Fig. 6a diffusion data for undoped YAG single-crystal. From these results, it can be noticed that the volume diffusion data obtained for YAG single-crystals and polycrystals exhibit fairly good agreement in terms of activation energy. The slight discrepancy between D_v values could be inferred to different amounts of extrinsic defects (dislocations, vacancies, interstitials, etc.) which would result from the synthesis way used for single and polycrystals. Since the activation energies are similar for YAG single- and polycrystals (643 ± 11 kJ mol^{-1} for polycrystalline YAG versus 561 ± 33 kJ mol^{-1} for single-crystal), it can be concluded that the same mechanism governs the bulk diffusion of neodymium in both single-crystal and polycrystalline YAG. Therefore, Cherniak[11] reported the same value ($Q_v = 567 \pm 15$ kJ mol^{-1}) in YAG single-crystals from Nd concentration profiles determined by means of RBS technique.

As reported in literature for ytterbium[9,10] and neodymium,[24] the bulk diffusion coefficient of the rare-earth element in polycrystalline YAG is about five orders of magnitude smaller than grain boundary diffusion coefficient. This trend is usually observed for polycrystalline materials. On the contrary, it is not usual to have similar activation energies for the bulk and grain boundary diffusion: indeed, the Q_{gb}/Q_v ratio is generally close to 0.8 in ceramics.[12] In this context, the difference between the neodymium grain boundary and bulk diffusivities should be correlated to the variations of the D_0 pre-exponential term in the Arrhenius law (see Eqs. (4) and (5)). This phenomenon could be explained by considering the grain boundaries as defects hosts, *i.e.* the zone where the formation or the segregation of cation (*e.g.* Al^{3+}, Y^{3+} or Nd^{3+}) vacancies could be favoured.[25,26] Thus, the increase of the point defects concentration along the YAG grain boundary could be linked to that of the D_0 term in the D_{gb} expression (Eq. (5)).

Moreover, the examination of the data reported in literature for Yb^{3+} diffusion in YAG polycrystals[9] reveals that these results are in accordance with those obtained during the present study

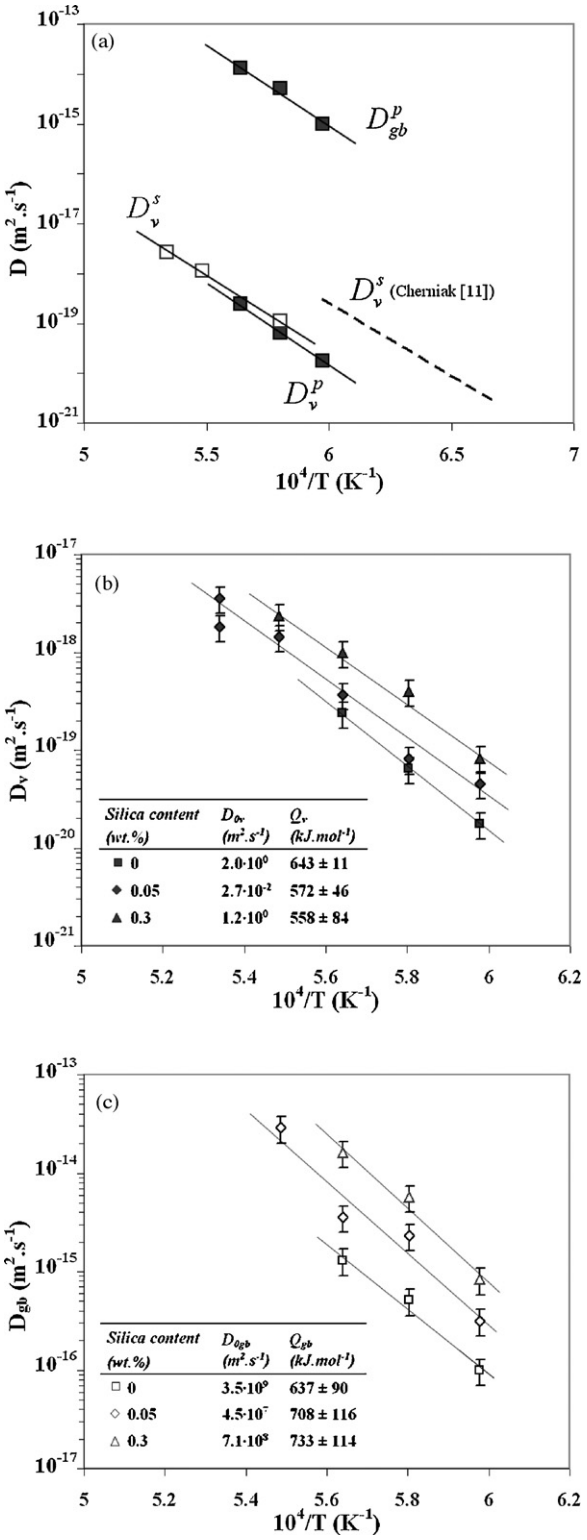

Fig. 6. (a) Arrhenius plot of Nd^{3+} volume and grain boundary diffusion coefficients (D_v^p and D_{gb}^p, respectively) for "pure" YAG polycrystals and volume diffusion coefficients for YAG single-crystal (D_v^s). Comparison with the volume diffusion data issued from Ref. [11]. Lattice (b) and grain boundary diffusivities (c) of Nd^{3+} in SiO_2-doped YAG versus reciprocal temperature.

for Nd^{3+} diffusion over the same temperature range. Nevertheless, a slight difference not larger than a factor of 10 was measured between the diffusivities of both cations (Yb^{3+} and Nd^{3+}). It is well known that the diffusivity scales with the inverse of the square root of mass.[21] As a consequence, the difference of the atomic mass between ytterbium and neodymium would lead to a difference in diffusivities by a factor of about 1.1 which remains within the experimental uncertainties. Otherwise, the valence state and size of the Yb^{3+} cations ($r_{Yb} = 0.098$ nm) which are similar to those of the Nd^{3+} cations ($r_{Nd} = 0.112$ nm)[19] do not allow to explain the discrepancy between diffusivities. Finally, the significant difference in average grain size for the starting sintered YAG samples (10 μm for the present study and 2 μm in Ref. [9]) could be responsible for the higher values of rare-earth cations diffusivities given by Jimenez-Melendo et al. in Ref. [9] compared to those reported in the present work.

3.2. The effect of silica addition

Fig. 6b shows the variation of neodymium lattice diffusion in YAG versus reciprocal temperature for different silica contents. The corresponding frequency factors D_0 and activation energies Q are also given. All the diffusion data obtained are reported in Table 1. From these results, it can be noted that similar activation energies for the bulk diffusion are determined whatever the silica content. However, the difference between the diffusivities reported in Fig. 6b appears to result from the frequency factor D_0 rather than from the activation energy term. From literature,[18,27–30] it is usually admitted that the preponderant intrinsic defects in the YAG lattice are the rare-earth cations and oxygen vacancies (V_{RE}''', $V_O^{\bullet\bullet}$) or antisites (Y_{Al}). It was also inferred that silicon cation would be mainly present on aluminum sites and not on yttrium ones because of the smaller size mismatch between Si^{4+} (0.026 nm) and Al^{3+} (0.039 nm).[18,19,31] Therefore, according to previous works,[32] the silicon solubility remains low in YAG and for instance it should not exceed 1.5 at.% at 1550 °C. The charge defects introduced by Si^{4+} tetravalent cations would be then compensated by the formation of yttrium vacancies (V_Y''') according to Eq. (1).[18,26,31] Otherwise, it has been suggested[33] that the rare-earth cation migration in YAG lattice is controlled by the mechanism of the REE cation jumping on Y^{3+} vacancies. As a consequence, the higher the silica content, the higher is the concentration of extrinsic cation vacancies and the higher is the neodymium cation diffusivity in the YAG host lattice.

The neodymium grain boundary diffusion coefficients determined for silica-doped YAG materials are reported in Fig. 6c and Table 1. Whatever the silica content, it can be seen that the grain boundary diffusivities of Nd^{3+} are about five orders of magnitude higher than the respective lattice diffusivities. This result highlights the grain boundaries as preferential paths for the rare-earth diffusion. Furthermore, the calculated activation energies were found to be comparable for both volume and grain boundary diffusion of Nd^{3+} in YAG whatever the silica content (see Fig. 6b and c). This result suggests that the same diffusion process for Nd^{3+} cation diffusion occurs when silica additions range between 0.05 and 0.3 wt.% in YAG.

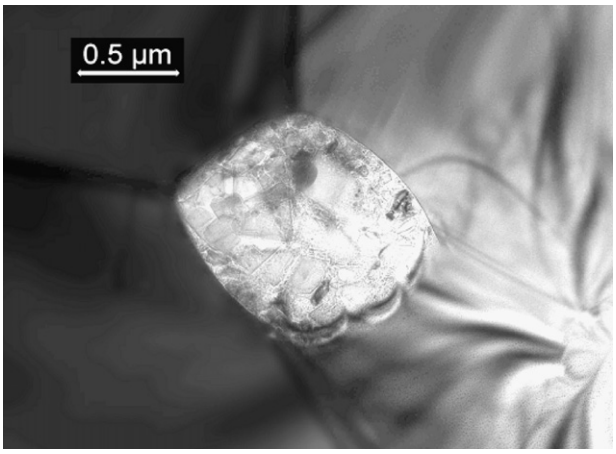

Fig. 7. TEM observation of an intergranular inclusion at triple point in YAG sample doped with 0.3 wt.% SiO_2 and sintered at 1700 °C for 15 min.

To explain the difference of the grain boundary diffusivities between undoped and silica-doped samples, one should consider the occurrence of intergranular inclusions at higher silica content (see Fig. 7). From further scanning transmission electron microscopy (STEM) coupled with energy dispersive X-ray spectroscopy (EDXS) analyses, these inclusions were analyzed as silica-rich secondary phases and were attributed to some residues from the liquid phase that forms at temperature higher than 1400 °C.[17] After sintering at 1700 °C for 3 h, no continuous thin film of interphase was evidenced from TEM investigations. Nevertheless, glassy pockets were detected at some triple points as shown in Fig. 7. This result is in fair agreement with a previous study[34] which showed that no distinct amorphous film could be identified by TEM imaging of such interfaces. However, the interface seemed to be highly perturbed and from both high-resolution electron microscopy (HREM) imaging coupled with EDXS analyses of such interfaces, these authors suggested that silicon segregates at YAG boundaries.

Otherwise, it can be worth to consider the effect of the grain size which depends on the silica content (see Table 1) on the Nd^{3+} grain boundary diffusion. It can be supposed that the increase of the silica content could enhance the grain boundary diffusion by rising the short-circuits concentration as reported in the literature for other systems.[21,26] To conclude, the silica addition allows improving the kinetic of the Nd^{3+} migration either by decreasing the average grain size of sintered YAG materials or by leading to the appearance of a silica-enriched liquid phase at the grain boundary.

4. Implications for Nd:YAG sintering

4.1. Densification mechanism for silica-free Nd:YAG samples

In a previous study,[35] a generalized model with a single equation of the instantaneous densification rate has been employed to quantify the solid-state sintering of the undoped Nd:YAG as a continuous process from the beginning to the end. The analytical treatment of the densification data obtained between 1450 and 1550 °C for the intermediate stage of the Nd:YAG sintering allowed to suppose that the densification should be controlled by the grain boundary diffusion.

In this context, the data obtained during the rare-earth cation diffusion experiments have significant implications to elucidate properly the densification mechanism of undoped Nd:YAG. Indeed, the activation energy of densification should be comparable with the activation energy for the grain-boundary diffusion of Nd^{3+} ($637 \pm 90\,kJ\,mol^{-1}$ (this study) or Y^{3+} ($530 \pm 190\,kJ\,mol^{-1}$).[9] Since the activation energy of the grain boundary diffusion for the other ionic species in YAG (Al^{3+} and O^{2-}) is significantly lower ($\approx 400\,kJ\,mol^{-1}$),[11,36] it is concluded that the densification mechanism during the intermediate stage of solid-state sintering of Nd:YAG is controlled by the grain boundary diffusion of the rare-earth cation (Y^{3+} or Nd^{3+}).

4.2. Grain growth mechanism for silica-doped Nd:YAG samples

During the intermediate or the final stage of the liquid-phase sintering (*e.g.* for the sintering of SiO_2 doped Nd:YAG specimens), densification slows down and microstructural coarsening by the Ostwald ripening-mechanism can become the dominant process.[37] According to the Lifshitz, Slyozov, Wagner (LSW) theory, the growth of the average grain size G with time t is given by Eq. (6):

$$G^n - G_0^n = kt \tag{6}$$

where G_0 is the initial value of grain size, k is a temperature dependent parameter and the exponent n is dependent on the rate-controlling mechanism: $n = 3$ when diffusion through the liquid is the rate-limiting step, and $n = 2$ for rate control by the interface reaction.

A systematic study of the grain growth for silica-doped Nd:YAG ceramics was made while varying the temperature and the holding time. A previous study[17] has clearly reported that the liquid-phase sintering of Nd:YAG ceramics is operative between 1400 and 1550 °C. Consequently, the present 0.3 wt.% SiO_2 doped Nd:YAG specimens were sintered at different temper-

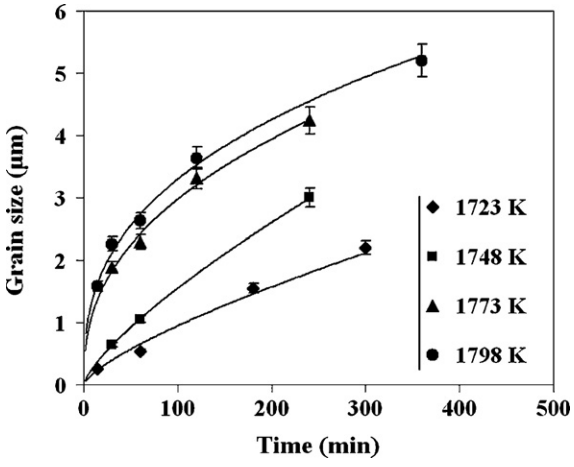

Fig. 8. Evolution of average grain size G versus soaking time for 0.3 wt.% silica-doped Nd:YAG samples between 1450 and 1525 °C.

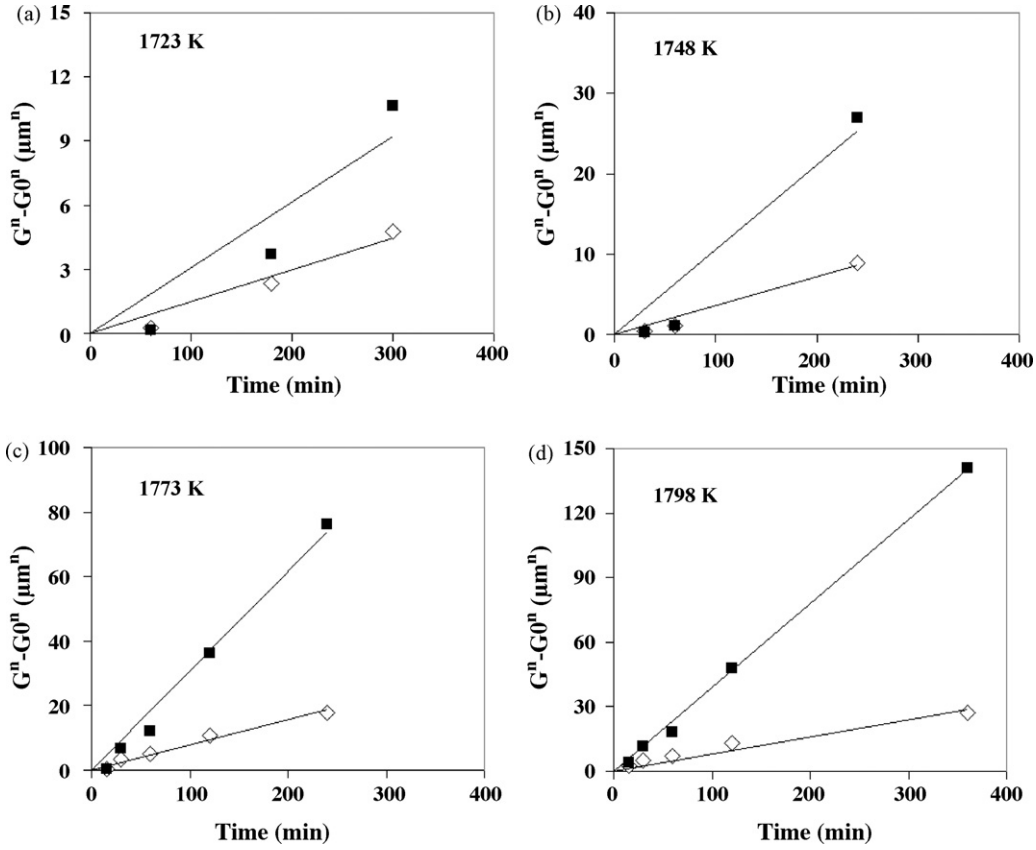

Fig. 9. Plot of $G^n - G_0^n$ function versus soaking time and straight line fits with $n=2$ (open symbol) or $n=3$ (closed symbol) for 0.3 wt.% silica-doped Nd:YAG samples at 1450 °C (a), 1475 °C (b), 1500 °C (c) and 1525 °C (d).

atures ranging between 1450 and 1525 °C and for dwell times varying between 15 min and 6 h. These thermal treatments can be correlated to the final stage of the Nd:YAG liquid-phase sintering with regards to the high relative density values (≥92% for the whole set of sintered samples).

The grain growth kinetics were established from the average grain size measurements as a function of soaking time and temperature and were reported in Fig. 8. It can be noticed the drastic increase of the average grain size with temperature at a given soaking time. Then, the $G^n - G_0^n$ function was plotted versus time (Fig. 9) for each soaking temperature and $n=2$ (open symbols and dotted lines) or $n=3$ (closed symbols and full lines). G_0 was chosen as being equal to 0.25 μm which corresponds to the mean grain size of YAG particles at 1400 °C (*i.e.* just after the reaction leading to the YAG phase and just before the formation of liquid phase[17]). Table 2 displays the R^2 coefficient values

Table 2
Linear regression coefficient (R2) determined from the grain growth data for different *n* exponent values.

Temperature (°C)	Linear regression coefficient (R2)	
	n = 2	*n* = 3
1450	**0.937**	0.856
1475	**0.959**	0.917
1500	0.974	**0.981**
1525	0.927	**0.998**

corresponding to a straight line fit, at different soaking temperatures and for the different *n* exponent values. From data reported in Table 2, it seems that the best straight line fit is obtained by assuming $n=2$ at low temperature ($T<1500$ °C). At higher temperature, the determination of the appropriate n value appears to be more complex because the R^2 coefficient values for both fits ($n=2$ and $n=3$) are very close (see Table 2). Nevertheless, the hypothesis of *n* equal to 3 could be retained especially when the sintering temperature would reach 1525 °C. Consequently, these results would suggest that the diffusion-controlled coarsening could become commonly active at higher temperature whereas the interface reaction could be the rate-limiting step at lower temperature.

Otherwise, the *k* parameter values determined from the plots of Fig. 9 were reported as a function of reciprocal temperature. From this Arrhenius diagram (Fig. 10), the apparent activation energies E_a of the grain growth are equivalent to 880 and 250 kJ mol^{-1} at low and high temperature, respectively. First, it can be noticed that these latter values are not in accordance with the apparent activation energy determined for the REE grain boundary and bulk diffusion at the same temperature. So, the reaction at the liquid/grain interface would govern the grain growth kinetic at the lower temperature, as supported by the good agreement between the present E_a values with those reported in literature for the enthalpy of solution of rare-earth oxides.[38] Moreover, E_a value at higher temperature (*i.e.* 250 kJ mol^{-1}) seems to be consistent with the aluminum and REE cations dif-

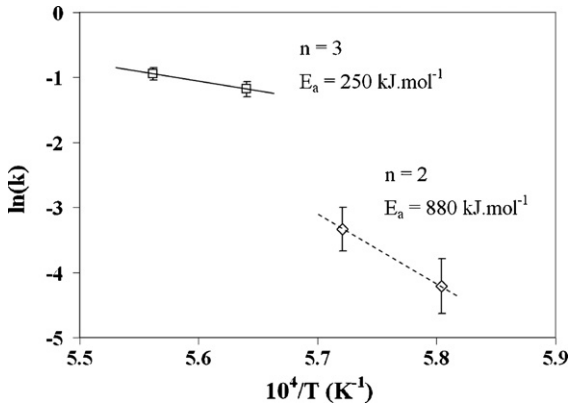

Fig. 10. Arrhenius plot of the (k) kinetical constant values for the grain growth determined from Fig. 9.

fusion (Nd^{3+}, Y^{3+} or Al^{3+}) in aluminosilicate or yttriosilicate glasses which activation energies have been reported inferior to 350 kJ mol^{-1}.[39–41]

5. Conclusion

The neodymium lattice and grain boundary diffusion coefficients were determined by a dip-coating method coupled with SIMS analyses, as a function of the annealing temperature and silica content. For the undoped Nd:YAG polycrystalline specimens, all the data so-obtained are consistent with the hypothesis that the Nd^{3+} diffusion should be controlled by the diffusion of yttrium cation (Y^{3+}) *via* a vacancy mechanism in YAG. Even if the diffusion mechanism seems to be invariant whatever the SiO_2 content in Nd:YAG, silica addition was found to enhance neodymium diffusivity by a factor 10. This effect could be explained through the formation of extrinsic defects as rare-earth vacancies (*i.e.* V_Y''') resulting from the silicon solubility in the YAG lattice.

By using the kinetic data issued from the diffusion experiments, the mechanisms of the densification and the grain growth have been investigated during the intermediate or the final stage of the sintering for undoped or silica-doped Nd:YAG ceramics. It appeared that the densification process during the intermediate stage of the solid-state sintering of the undoped Nd: YAG is controlled by the rare-earth grain boundary diffusion with an activation energy of 595 kJ mol^{-1}. Therefore, the grain growth kinetics during the final stage of the Nd:YAG liquid-phase sintering (*i.e.* with silica additions) obey to an Ostwald ripening-mechanism. It was observed that the rate-limiting step of the grain growth depends on the soaking temperature: at low temperature ($\leq$1500 °C), the interface reaction could be considered as the rate-controlling process whereas at higher temperature, the coarsening mechanism should be governed by the REE or aluminum cations diffusion through the liquid phase.

Acknowledgments

The authors are grateful to Dr. Bernard Soulestin and Valérie Coudert (SPCTS, UMR CNRS 6638, University of Limoges, France) for TEM samples preparation, sintering treatments and AFM observations, respectively.

The authors are also pleased to thank to Dr. Jaafar Ghanbaja (LCSM-Service Commun de Microscopie, CNRS UMR 7555, University of Nancy, France) for TEM analyses.

References

1. Ikesue, A., Kinoshita, T., Kamata, K. and Yoshida, K., Fabrication and optical properties of high-performance polycrystalline Nd:YAG ceramics for solid-state lasers. *J. Am. Ceram. Soc.*, 1995, **78**, 1033–1040.
2. Yagi, H., Yanagitani, T., Numazawa, T. and Ueda, K. I., The physical properties of transparent $Y_3Al_5O_{12}$ elastic modulus at high temperature and thermal conductivity at low temperature. *Ceram. Int.*, 2007, **33**, 711–714.
3. De With, G., Preparation, microstructure and properties of $Y_3Al_5O_{12}$ ceramics. *Philips J. Res.*, 1987, **42**, 119–130.
4. De With, G. and Parren, J. E. D., Translucent $Y_3Al_5O_{12}$ ceramics: mechanical properties. *Solid State Ionics*, 1985, **16**, 87–94.
5. Yagi, H., Yanagitani, T., Takaichi, K., Ueda, K. I. and Kaminskii, A. A., Characterizations and laser performances of highly transparent Nd^{3+}:$Y_3Al_5O_{12}$ laser ceramics. *Opt. Mater.*, 2007, **29**, 1258–1262.
6. Lu, J., Yagi, H., Takaichi, K., Uematsu, T., Bisson, J.-F., Feng, Y. *et al.*, 110 W ceramic Nd^{3+}:$Y_3Al_5O_{12}$ laser. *Appl. Phys.*, 2004, **B79**, 25–28.
7. Liu, Q., Gong, M., Lu, F., Gong, W., Li, C. and Ma, D., Corner-pumped Yb: yttrium aluminum garnet slab laser emitted up to 1 kW. *Appl. Phys. Lett.*, 2006, **88**, 101113.
8. Lu, J., Ueda, K. I., Yagi, H., Yanagitani, T., Akiyama, Y. and Kaminskii, A. A., Neodymium doped yttrium aluminum garnet ($Y_3Al_5O_{12}$) nanocrystalline ceramics—a new generation of solid state laser and optical materials. *J. Alloys Compd.*, 2002, **341**, 220–225.
9. Jimenez-Melendo, M., Haneda, H. and Nozawa, H., Ytterbium cation diffusion in yttrium aluminum garnet (YAG)—implications for creep mechanisms. *J. Am. Ceram. Soc.*, 2001, **84**, 2356–2360.
10. Haneda, H., Miyazawa, Y., Sakaguchi, I., Nozawa, H., Yanagitani, T. and Jimenez-Melendo, M., Diffusion of scandium, gallium and ytterbium ions into single- and polycrystalline yttrium aluminum garnets. *J. Ceram. Soc. Jpn.*, 2001, **109**, 114–121.
11. Cherniak, D. J., Rare earth element and gallium diffusion in yttrium aluminum garnet. *Phys. Chem. Minerals*, 1998, **26**, 156–163.
12. Swaroop, S., Kilo, M., Argirusis, C., Borchardt, G. and Chokshi, A. H., Lattice and grain boundary diffusion of cations in 3YTZ analyzed using SIMS. *Acta Mater.*, 2005, **53**, 4975–4985.
13. De With, G., Translucent $Y_3Al_5O_{12}$ ceramics. *Mater. Res. Bull.*, 1984, **19**, 1669–1674.
14. Vrolijk, J. W. G. A., van dem Cruisem, S. and Metselaar, R., The influence of MgO and SiO_2 dopants on the sintering behaviour of yttrium aluminum garnet ceramics. *Ceram. Trans.*, 1995, **51**, 573–577.
15. Ikesue, A., Yoshida, K., Yamamoto, T. and Yamaga, Y., Optical scattering centers in polycrystalline Nd:YAG laser. *J. Am. Ceram. Soc.*, 1997, **80**, 1517–1522.
16. Kochawattana, S., Stevenson, A., Lee, S. H., Ramirez, M., Gopalan, V., Dumm, J., Castillo, V. K., Quarles, G. J. and Messing, G. L., Sintering and grain growth in SiO_2 doped Nd:YAG. *J. Eur. Ceram. Soc.*, 2008, **28**, 1527–1534.
17. Maître, A., Sallé, C., Boulesteix, R., Baumard, J.-F. and Rabinovitch, Y., Effect of silica on the reactive sintering of polycrystalline Nd:YAG ceramics. *J. Am. Ceram. Soc.*, 2008, **91**, 406–413.
18. Kuklja, M., Defects in yttrium aluminum perovskite and garnet crystals: atomistic study. *J. Phys.: Condens. Matter*, 2000, **12**, 2953–2967.
19. Shannon, R. D. and Prewitt, C. T., Effective ionic radii in oxides and fluorides. *Acta Crystallogr.*, 1969, **B25**, 925–946.
20. Pontes, F. M., Longo, E., Rangel, J. H., Bernardi, M. I., Leite, E. R. and Varela, J. A., $Ba_{1-x}Sr_xTiO_3$ thin films by polymeric precursor method. *Mater. Lett.*, 2000, **43**, 249–253.
21. Philibert, J., *Atom Movements: Diffusion and Mass Transport in Solids*. Les Editions de Physique, Les Ulys, France, 1991.

22. Le Claire, A. D., The analysis of grain boundary diffusion measurements. *Brit. J. Appl. Phys.*, 1963, **14**, 351–356.
23. Klimm, D., Ganschow, S., Pajaczkowska, A. and Lipinska, L., On the solubility of Nd^{3+} in $Y_3Al_5O_{12}$. *J. Alloys Compd.*, 2007, **436**, 204–208.
24. Yagi, H., Takaichi, K., Ueda, K. I., Yamasaki, Y., Yanagitani, T. and Kaminskii, A. A., The physical properties of composite YAG ceramics. *Laser Phys.*, 2005, **15**, 1338–1344.
25. Dieckamann, R., Point defects and transport in non-stoichiometric oxides: solved and unsolved problems. *J. Phys. Chem. Solids*, 1998, **59**, 525–597.
26. Badrour, L., Moya, E. G., Bernadini, J. and Moya, F., Fast diffusion of silver in single and polycrystals of a-alumina. *J. Phys. Chem. Solids*, 1989, **50**, 551–561.
27. Hayes, W., Yamaga, M., Robbins, D. J. and Cockayne, B., Optical detection of EPR of recombination centres in YAG. *J. Phys.*, 1980, **C13**, L1085–L1089.
28. Rotman, S. R. and Warde, C., Defect luminescence in cerium-doped yttrium aluminum garnet. *J. Appl. Phys.*, 1985, **58**, 522.
29. Milanese, C., Buscaglia, V., Maglia, F. and Anselmi-Tamburini, U., Disorder and nonstoichiometry in synthetic garnets $A_3B_5O_{12}$ (A = Y, Lu–La, B = Al, Fe, Ga). A simulation study. *Chem. Mater.*, 2004, **16**, 1232–1239.
30. Selim, F. A., Solodovnikov, D., Weber, M. H. and Lynn, K. G., Identification of defects in $Y_3Al_5O_{12}$ by position annihilation spectroscopy. *Appl. Phys. Lett.*, 2007, **91**, 104105.
31. Stanek, C. R., McClellan, K. J., Levy, M. R. and Grimes, R. W., Extrinsic defect structure of $RE_3Al_5O_{12}$ garnets. *Phys. Status Solidi*, 2006, **B243**, 75–77.
32. Sun, W. Y., Li, X. T., Ma, L. T. and Yen, T. S., Solubility of Si in YAG. *J. Solid State Chem.*, 1984, **51**, 315–320.
33. Haneda, H., A study of defect structures in oxide materials by secondary ion mass spectrometry. *Appl. Surf. Sci.*, 2003, **203**, 625–629.
34. Ikesue, A., Aung, Y. L., Yoda, T., Nakayama, S. and Kamimura, T., Fabrication and laser performance of polycrystal and single crystal Nd:YAG by advanced ceramic processing. *Opt. Mater.*, 2007, **29**, 1289–1294.
35. Boulesteix, R., Maître, A., Baumard, J.-F., Sallé, C. and Rabinovitch, Y., and Rabinovitch Y., Mechanism of the liquid-phase sintering for Nd:YAG ceramics. *Opt. Mater.*, 2009, **31**, 711–715.
36. Sakaguchi, I., Haneda, H., Tanaka, J. and Yanagitani, T., Effect of composition on the oxygen tracer diffusion in transparent yttrium aluminum garnet (YAG) ceramics. *J. Am. Ceram. Soc.*, 1996, **79**, 1627–1632.
37. Rahaman, M. N., *Sintering of Ceramics*. CRC Press Edition, New York, 2008, pp. 181–215.
38. Zhang, Y., Navrotsky, A., Li, H., Li, L., Davis, L. L. and Strachan, D. M., Energetics of dissolution of Gd_2O_3 and HfO_2 in sodium aluminoborosilicate glasses. *J. Non-Cryst. Solids*, 2001, **296**, 93–101.
39. Kwon, O. H. and Messing, G. L., Kinetic analysis of solution-precipitation during liquid-phase sintering of alumina. *J. Am. Ceram. Soc.*, 1990, **73**, 275–281.
40. Liang, Y., Cherniak, D. J., Morgan, Z. T. and Hess, P. C., Eu^{2+} and REE^{3+} diffusion in enstatite, diopside, anorthite, and a silicate melt: a database for understanding kinetic fractionation of REE in the lunar mantle and crust. *Lunar Planetary Sci.*, 2004, **XXXV**, 1894.
41. Jean, J. H. and Gupta, T. K., Densification kinetics and modeling of glass-filled alumina composite. *J. Mater. Res.*, 1994, **9**, 771–780.